Original Research Article, SPECIAL ISSUE *Enantioseparation 2022*

Unravelling functions of halogen substituents in the enantioseparation of halogenated planar chiral ferrocenes on polysaccharide-based chiral stationary phases: experimental and electrostatic potential analyses

Barbara Sechi,[a,‡] Alessandro Dessì,[a,‡] Carlo Gatti,[b] Roberto Dallocchio,[a] Bezhan Chankvetadze,[c] Sergio Cossu,[d] Victor Mamane,[e,*] Patrick Pale,[e] and Paola Peluso[a,*]

[a] Istituto di Chimica Biomolecolare ICB, CNR, Sede secondaria di Sassari, Traversa La Crucca 3, Regione Baldinca, I-07100 Li Punti - Sassari, Italy

[b] CNR-SCITEC, Istituto di Scienze e Tecnologie Chimiche "Giulio Natta", sezione di via Golgi, via C. Golgi 19, 20133 Milano, Italy

[c] Institute of Physical and Analytical Chemistry, School of Exact and Natural Sciences, Tbilisi State University, Chavchavadze Ave 3, 0179 Tbilisi, Georgia

[d] Dipartimento di Scienze Molecolari e Nanosistemi DSMN, Università Ca' Foscari Venezia, Via Torino 155, I-30172 Mestre Venezia, Italy

[e] Institut de Chimie de Strasbourg, UMR CNRS 7177, Equipe LASYROC, 1 rue Blaise Pascal, 67008 Strasbourg Cedex, France

* Corresponding authors. E-mail address: paola.peluso@cnr.it (Paola Peluso); vmamane@unistra.fr (Victor Mamane)

‡ These authors contributed equally to this work

ABSTRACT

Planar chiral halogenated ferrocenes have come in useful as synthetic intermediates over the years, allowing for the preparation of functionalized derivatives for catalysis, material science, optoelectronics, and medicinal chemistry. Despite their chemical interest, few halogenated planar chiral ferrocenes have been prepared in enantiopure form by asymmetric synthesis so far. Enantioselective HPLC on polysaccharide-based chiral stationary phases (CSPs) has been used for resolving planar chiral ferrocenes making both enantiomers available. However, the enantioseparation of derivatives containing halogens or alkyl groups exclusively remains rather challenging. Given this context, in this study the enantioseparation of eleven dihalogenated planar chiral ferrocenes was systematically explored by using

five polysaccharide-based CSPs under multimodal elution conditions. Baseline enantioseparations were achieved for nine analytes with separation factors (α) ranging from 1.15 to 1.66. Thermodynamic quantities associated with the enantioseparations were derived from van't Hoff plots, and for 1-halo-2-(iodoethynyl)ferrocenes (1-halogen = F, Cl, Br) halogen-dependent thermodynamic profiles were identified on a cellulose *tris*(3,5-dimethylphenylcarbamate)-based column. The impact of CSP structure and mobile phase (MP) polarity on the enantioseparation was evaluated. In addition, with the aim to unravel the functions of halogen substituents in mechanisms and noncovalent interactions underlying selector-selectand complex formation at molecular level, local electron charge density of specific molecular regions of the interacting partners were evaluated in terms of calculated electrostatic potential (*V*) and related source function (SF) contributions. On this basis, the impact of halogen type and position on the enantioseparation was investigated by correlating theoretical and experimental data.

Keywords: Electrostatic potential, Enantioseparation, Halogen bond, Polysaccharide-based chiral stationary phases, Source function

1. Introduction

The serendipitous discovery of ferrocene in 1951 [1, 2] and its structural determination a year later [3-5] have initiated an ever-increasing number of researches, which have led to the synthesis of numerous substituted ferrocenyl derivatives for various applications, from fuel additive and electrochemistry to catalysis, medicinal chemistry, optoelectronics, and material sciences [6-8]. Haloferrocenes were among the first of these derivatives [9], at first in exploratory works but also in attempts to reach the elusive ferrocyne, analog to benzyne [10, 11]. Since, halogenated ferrocenes have appeared as key intermediates for accessing polysubstituted ferrocenes [12]. More recently, iodinated ferrocenes turned out to be involved in halogen bond (XB) in solid state [13, 14], and even in solution with emerging application as organocatalyst in organic synthesis [13, 15].

Due to the peculiar ferrocene structure, halogenated and other substituted ferrocenes exhibit planar chirality depending on the substitution pattern. Monosubstituted ferrocenes are prochiral compounds, while different disubstitution on one ferrocene ring leads to planar chirality. Such phenomenon has led to the huge development of ferrocenyl derivatives as chiral ligands in asymmetric synthesis and catalysis [8,16]. However, only a few enantiomerically enriched haloferrocenes are known [17-20].

Although asymmetric synthesis procedures for accessing enantiomerically enriched halogenated ferrocenes are available, enantiomeric purity is not always satisfactory [21]. An alternative could be the resolution of planar chiral ferrocenes through enantioselective HPLC on polysaccharide-based chiral stationary phases (CSPs). However, while moderate to high enantioselectivities were obtained under normal-phase (NP) elution conditions for ferrocenes bearing polar substituents [19,20,22], the enantioseparation of derivatives containing halogens or alkyl groups exclusively remains rather challenging [23-25].

Given the interest in the chemistry of halogenated ferrocenes, and especially of planar chiral ones, we reported herein a systematic study on the HPLC enantioseparability of ferrocenes **1**-**11** (Fig. 1) by using five polysaccharide-based CSPs (Table S1, Supplementary data) under multimodal elution conditions.

For some halogenated ferrocenes, the effect of temperature on the enantioseparations was considered, and thermodynamic quantities associated with the enantioseparations were derived from van't Hoff plots.

A second aim of this study was to evaluate the functions of halogen substituents on the enantioseparation [26], exploring the possibility of XB-based enantiorecognition mechanisms [27,28]. For this purpose, electrostatic potential values, mapped on electron density isosurfaces (V_S) and associated with the main interaction sites of selectors and of compounds **1**–**11**, were calculated and correlated with the chromatographic parameters [29]. In addition, with the aim of theoretically explaining the origin and trends of the calculated V values, the source function (SF) reconstruction of V was also applied [30-32]. Recently, this theoretical approach has provided insights into the stereoelectronic features underlying the interaction capability of selectands in LC analyses [31-33].

2. Materials and methods

2.1. Chemicals

Compounds **1**-**11** were prepared and characterized as previously reported [15,34-36]. HPLC grade *n*-hexane (Hex), methanol (MeOH), 2-propanol (2-PrOH), and water were purchased from Sigma-Aldrich (Taufkirchen, Germany).

2.2. Chromatography

An Agilent Technologies (Waldbronn, Germany) 1100 Series HPLC system (high-pressure binary gradient system equipped with a diode-array detector operating at multiple wavelengths (220, 254, 280, 360 nm), a programmable autosampler with a 20 µl loop, and a thermostated column compartment) was employed. Data acquisition and analyses were carried out with Agilent Technologies ChemStation Version B.04.03 chromatographic data software. The UV absorbance is reported as milliabsorbance units (mAU). Lux Cellulose-1 (C-1) (cellulose *tris*(3,5-dimethylphenylcarbamate), CDMPC), Lux i-Cellulose-5 (iC-5) (cellulose *tris*(3,5-dichlorophenylcarbamate), CDCPC), Lux Amylose-1 (A-1) and Lux i-Amylose-1 (iA-1) (amylose *tris*(3,5-dimethylphenylcarbamate), ADMPC), and Lux i-Amylose-3

(iA-3) (amylose *tris*(3-chloro-5-methylphenylcarbamate), ACMPC) (5 μm) (Phenomenex Inc., Torrance, CA, USA), were used as chiral columns (250 × 4.6 mm). Analyses were performed in isocratic mode at 25°C if not indicated otherwise. The flow rate (*FR*) was set at 0.8 ml/min. For compounds **1**, **3**, and **6**, the enantiomer elution order (EEO) was determined by injecting enantiomers of known absolute configuration [15]. For compounds **2**, **4**, **5**, and **7**-**11**, the relative EEO was assigned by injecting pure enantiomers of unknown absolute configuration which are denoted as $X_{\text{compound number}}$ and $Y_{\text{compound number}}$. The van't Hoff experiments were conducted at 5, 10, 15, 20, 25, 30, 35, and 40 °C by using a thermostat jacket equipped with a RE104 LAUDA circulating water-bath (Lauda, Königshofen, Germany) (resolution 0.1 °C; accuracy ±0.4 °C; temperature control ±0.02 °C). When the temperature was changed, the column was allowed to equilibrate for 1 h before injecting the samples. Thermodynamic parameters were derived from the slopes and the intercepts of the van't Hoff plots by linear regression analysis (see Supplementary data for details). Statgraphics Centurion XVI (Statpoint Technologies, Inc., Warrenton, VA, USA) was used for all linear regression analyses.

2.3. Computations

Electrostatic potential extrema on the molecular electron density isosurfaces (maxima and minima) ($V_{S,max}$ and $V_{S,min}$) (au, electrons/bohr) were calculated by using Gaussian 09 (Wallingford, CT 06492 USA) [37], at the density functional theory (DFT) level of theory using the B3LYP functional and the def2TZVPP basis set. Search for the exact location of $V_{S,max}$ and $V_{S,min}$ was made through the Multiwfn code [38] and through its module enabling quantitative analyses of molecular surfaces (isovalue 0.002 au) [39]. Theory and details of the SF reconstruction of V_S are available in the Supplementary data. The results of the SF decomposition of $V_{S,extrema}$ are described on the basis of the equations (1,2) for compounds **1**-**6** and **7**-**11**, respectively, with X = F, Cl, Br and Cp = cyclopentadienyl.

$$V_{S,extrema} = SF(I) + SF(X) + SF(Fe) + SF(C{\equiv}C) + SF(Cp_{substituted}) + SF(Cp_{unsubstituted}) \quad (1)$$

$$V_{S,extrema} = SF(I) + SF(X) + SF(Fe) + SF(Cp_{substituted}) + SF(Cp_{unsubstituted}) \quad (2)$$

3. Results and discussion

3.1. Conceptual basis: integrating experimental and electrostatic potential analyses

With the twofold purpose of *i)* improving methods to enantioseparate halogenated ferrocenes, and *ii)* unravelling enantioseparation mechanisms at the molecular level, the impact of analytes and CSP structures, and of mobile phase (MP) polarity on retention (k) and separation (α) factors was explored. CSPs, and MPs and analytes were selected on the basis of the following remarks:

a) the performances of different polysaccharide selectors were evaluated, and compared in terms of polysaccharide backbone (cellulose-based C-1 vs. amylose-based A-1), and of type of carbamate pendant groups (methylated A-1, iA-1, C-1 vs. chlorinated iC-5 vs. methylated and chlorinated iA-3) (Table S1, Supplementary data). The electronic properties of the carbamate moiety, which are tuned by methyl and chlorine substituents located on the phenyl ring of the carbamate pendant groups, were determined by DFT calculations (Table S2, Supplementary data). The impact of the anchoring technique (immobilization vs. coating) was also considered by comparing the performances of amylose *tris*(3,5-dimethylphenylcarbamate) (ADMPC)-based columns (A-1 *versus* iA-1) [40,41];

b) under multimodal elution conditions, the effect of MP on the enantioseparations was comparatively evaluated by using Hex/2-PrOH 95:5 v/v (A), Hex/2-PrOH/MeOH 95:2.5:2.5 v/v/v (B), MeOH 100% (C), MeOH/water 95:5 v/v (D), and MeOH/water 90:10 v/v (E). In particular, the comparative use of A-E, as MPs, allowed for evaluating the effect of increasing hydrophobicity of the medium. In addition, MeOH can perform different functions depending on its concentration in the MP. The use of pure MeOH (C) impacts the intramolecular hydrogen bonds (HBs) determining the highly-ordered structure of the polysaccharide, thus producing a huge effect within the polysaccharide structure [42-44]. With MeOH, hydrophobic interactions tend to be more favoured compared to HBs, and the addition of water was expected to enhance hydrophobic interactions and increase capacity factors in accordance with a typical reversed-phase (RP) system [45]. In contrast, 2.5% MeOH (B) does not affect the highly-ordered three-dimensional structure of the polysaccharide. Rather, it may allow for fine tuning of the binding between

analyte and polysaccharide-based selector by favouring a better penetration of the analyte into the groove, and modulating hydrophobic *versus* HB interactions [42,43]. On this basis, methanol-containing MPs were shown to favour the enantioseparation of non-polar ferrocenes [25].

c) within the 1-halo-2-iodoethynyl (**1**-**3**), 1-halo-3-iodoethynyl (**4**-**6**), 1-halo-2-iodo (**7**-**9**), and 1-halo-3-iodo (**10**,**11**) ferrocene series (Fig. 1), the impact on enantioseparation of the substitution pattern (1,2-disubstituted: **1**-**3**, **7**-**9** vs 1,3-disubstituted: **4**-**6**, **10**, **11**), of the C≡C framework (**1**-**6** vs **7**-**11**), and of the distinctive halogen atom (F: **1**, **4**, **7**, **10**; Cl: **2**, **5**, **8**, **11**; Br: **3**, **6**, **9**) was evaluated. In compounds **1**-**11**, bound halogens may behave as (Fig. 2) *a)* HB and XB acceptors (I < Br < Cl < F) through the region of higher electron density, which forms a belt orthogonal to the C–X covalent bond, *b)* XB donor (I > Br > Cl > F) through the region of electron charge density depletion (σ-hole) located on the elongation of the C–X covalent bond, *c)* hydrophobic centres (I > Br > Cl > F), and *d)* bulky groups participating in repulsive interactions, in particular the heavy halogens such as Br (radius = 1.85 Å [46]) and I (radius = 1.98 Å [46]). In addition, the C≡C electronic cloud may function as HB acceptor, and the ferrocene Cp π-clouds have also electron donor properties. Then, ferrocene may be considered a three-dimensional analogue of the flat benzene ring [23], and its "barrel shape" offers better possibility for filling hydrophobic cavities compared to aryl and heteroaryl rings [47].

With the aim of exploring the interaction capability of compounds **1**-**11**, the local electron charge density of specific molecular regions of the analytes was investigated in terms of calculated V_S extrema, $V_{S,max}$ and $V_{S,min}$ (Fig. 2 and Table S3, Supplementary data), which are associated with electrophilic and nucleophilic regions, respectively. Moreover, the $V_{S,max}$ and $V_{S,min}$ values may be envisaged as being due to SF contributions from atoms or groups of the system by extending the Bader–Gatti SF for the electron density to *V*, as previously reported [31-33,48]. Thus, the decomposition of *V* in atomic or group contributions was considered in order to quantify the impact of single contributions to the *V* value (Tables S4-S13, Supplementary data). On this basis, the factors determining a certain *V* in a point could be inspected, attempting to disclose the fine reasons at the molecular level of the observed

chromatographic trends in series of structurally related compounds. It is reasonable to hypothesize that distinct molecular points may behave differently in noncovalent interactions if they present different SF contribution patterns, even if they also present similar *V* values at these points. Indeed, different SF contributions may reveal different capabilities of the overall molecule to rearrange electron charge density, stabilizing/destabilizing the system, after the perturbation of the electron charge density in a point due to the noncovalent contact. The source sign associated with $V_{S,max}$ contribution is positive or negative whether the atomic (or group) source concurs or opposes to the positive potential, whereas the opposite occurs for the $V_{S,min}$ contributions.

3.2. Chromatographic screening

The enantioseparation of the halogenated analytes **1**-**11** was examined by using twenty-five chromatographic systems generated by the combination of C-1, iC-5, A-1, iA-1, and iA-3, as CSPs, with A-E as MPs (Tables S14-S24, Supplementary data). A-1 and iA-3 showed better enantioseparation versatility toward ferrocenes **1**-**11** compared to C-1, iC-5 and iA-1, and seven and five compounds could be baseline resolved on these two columns, respectively. On the contrary, iC-5 exclusively provided partial enantioseparation of compound **1**, with low selectivity factors under normal phase (NP) elution conditions (A: $\alpha = 1.09$; B: $\alpha = 1.06$) (Table S14, Supplementary data). The immobilized iA-1 also showed limited versatility, and it could only baseline enantioseparate compounds **10** and **11** by using methanol-containing MPs (**10**: B-E; **11**: D, E). For this series of enantioseparations (Tables S23 and S24), iA1 provided lower selectivity factors ($1.19 \leq \alpha \leq 1.24$) compared to those observed on the coated A1 ($1.37 \leq \alpha \leq 1.42$). As an exception, compound **10** was enantioseparated on iA1 by using mixture B, as MP, whereas it remained not separated on the coated A-1 under the same elution conditions. For the enantioseparations on A-1 and iA-3, the values of *k* and α are summarized in Figures 3 and 4, respectively, along with the data related to the enantioseparations on C-1, as reference term for comparison.

Baseline enantioseparations were obtained at 25 °C for compounds **1**-**6**, **10**, and **11** with α values ranging from 1.15 to 1.66, whereas the best partial enantioseparations were obtained for **7** (α = 1.09), **8** (α = 1.09) and **9** (α = 1.07) by using the systems iA-3/B, C-1/E, and C-1/A, respectively. In all cases, the best selectivity values were obtained by using A-1 and iA-3 as CSPs with methanol-containing MPs, with the exception of compounds **8** and **9** which showed better enantioseparation on C-1. Compound **3** could be also baseline enantioseparated by using C-1 with mixture A as MP, but with a lower selectivity factor (α = 1.16) compared to that obtained with the system A-1/E (α = 1.21). Given that temperature impacts the chromatographic behaviour of the analytes in HPLC enantioseparation, it was considered as a variable to optimize separation [41,49,50], and the dependence of the enantioseparation on the temperature was also explored. On this basis, baseline enantioseparations could be also achieved for compound **8** with the system C1/E at 5 °C ($\alpha_{25°C}$ = 1.09→$\alpha_{5°C}$ = 1.22). Enantioseparation was also improved for **7** (α = 1.12) and **9** (α = 1.13) by using C-1 at 5 °C with the mixtures A and E, respectively. Nevertheless, baseline enantioseparations were not obtained in both cases. For compound **3**, selectivity with the system A-1/E could be improved by changing the operative temperature from 25 °C (α = 1.21) to 10 °C (α = 1.30). The chromatographic traces of representative baseline enantioseparations of compounds **1**-**11** are depicted in Figure S1 (Supplementary data).

Several cases of enantiomer elution order (EEO) reversal could be observed at 25 °C (Table 1), which are dependent on polymer backbone (**5**, **6**, **7**: C-1/B→A-1/B), pendant groups (**1**: C-1/A→iC-5/A; **1**, **3**: A1/E→iA-3/E), MP (**2**: C-1/B→C-1/E; **8**, **9**: C-1/A→C-1/D,E) and distinctive halogen type (C-1/A: **1**→**3**) and position (A-1/C,D,E: **3**→**6**) in the analyte. No reversal of the EEO was observed for compounds **4**, **10**, and **11**.

3.3. Effect of the selector structure on the enantioseparation

The columns used in this study contain selectors based on amylose and cellulose backbones. The native polymers are derivatized with chloro- or/and methyl-substituted phenylcarbamate pendant groups determining the distinctive stereoelectronic properties of each selector (Table S1, Supplementary data)

[40]. The amylose-based columns provided baseline enantioseparation for eight compounds (**1**-**6**, **10**, **11**), whereas only two compounds (**3**, **8**) were baseline enantioseparated with cellulose-based selectors. The column performances, in terms of number of baseline enantioseparations, decreased following the order A-1 (7) > iA-3 (5) > C-1 (2) > iC-5 (0). Two factors could contribute to this trend:

a) chiral cavity size: amylose-based selectors present a more compact structure with respect to the cellulose-based selectors [51]. Moreover, the introduction of chlorine increases the fraction of free N–H groups available for selector-analyte interactions [43], whereas the fraction of N–H involved in intramolecular HBs, contributing to maintain the highly-ordered structure of the CSP, decreases. This could produce for the chlorinated CSPs (iC-5 and iA-3) a wider cavity with respect to the dimethylated selectors, the overall enantioseparation resulting from the balance of carbamate polarity and intramolecular HB ability [43]. Thus, the dimension of the cavities inside the groove may be supposed to increase following the order A-1 < iA-3 < C-1 < iC-5. Consequently, more compact chiral cavities defined a better stereochemical environment for the enantiorecognition of halogenated ferrocenes **1**-**11**, favouring their enantioseparation, likely due to the small size of these ferrocene derivatives ($199 \leq$ volume ($Å^3$) ≤ 240). Selectivity values for baseline enantioseparations were generally higher for A-1 ($1.15 \leq \alpha \leq 1.66$) compared to iA-3 ($1.10 \leq \alpha \leq 1.41$).

b) pendant group structure: the effect of introducing chlorine in the CSP structure is to modify the electron charge density distribution on the pendant groups, thus the electron charge density on both C=O and phenyl ring decreases (π-acidity increases), whereas the acidity of the N–H increases [43,51]. Calculating $V_{S,max}$ and $V_{S,min}$ values on the amidic hydrogen and the carbonyl oxygen, respectively, located in the pendant groups of ADMPC (CDMPC) (C-1, A-1, iA-1), CDCPC (iC-5), and ACMPC (iA-3) confirmed this trend (Table S2, Supplementary data). Indeed, the $V_{S,max}$ and $V_{S,min}$ decreased following the order CDCPC (0.0990, -0.0536 au) > ACMPC (0.0914, -0.0595 au) > ADMPC (CDMPC) (0.0843, -0.0625). On this basis, given the higher performances of the ADMPC and CDMPC compared

to the ACMPC and CDCPC, respectively, the carbonyl oxygens seem to be important recognition sites for the ferrocene derivatives under investigation.

In almost all cases iA-1 showed lower enantioseparation ability compared to the coated A-1, thus the immobilization of the selector impacted on the column performances toward ferrocene **1**-**11**. The immobilized column exhibited good enantioseparation capability for compounds **10** and **11** exclusively, with methanol-containing MPs, thus under hydrophobic conditions. In this regard, it is worth mentioning that all the immobilization conditions produce chemical and/or physical alteration of the selector, and sometimes covalent immobilization technologies require the use of under-derivatized polysaccharides in order to attach the selector to the silica surface [40]. On the other hand, previous studies demonstrated that immobilization of ADMPC could impact the carbamate region, which is involved in HB interactions with the analytes, more than the substituted aromatic rings [41].

With the aim to compare the thermodynamic profiles of ADMPC, ACMPC, and CDMPC as selectors contained in A-1, iA-3, and C-1, respectively, by using mixture E as MP, temperature dependence of retention and selectivity was profiled for **1**-**6**, as representative compounds, in the range 5-40 °C (Tables S25-S34, Figs. S2-S7, Supplementary data). Thermodynamic quantities associated with the adsorption of analytes on the CSP surface were calculated from van't Hoff equations (Supplementary data for details). In this regard, it is worth highlighting that this type of analysis may be useful to inspect the nature of analyte/CSP association on the basis of thermodynamic considerations, but it does not allow for determining individually achiral and chiral features of enantioseparation and their actual ratio in the discrimination [52]. By using the thermodynamic ratio $Q = \Delta\Delta H°/(298\times\Delta\Delta S°)$ [53] as a parameter for comparison, the thermodynamic analysis evidenced in almost all cases an enthalpic contribution ($\Delta\Delta H°$) to the free energy difference ($\Delta\Delta G°$) associated to the enantioseparation increasing following the order C-1 ($1.00 \leq Q \leq 1.26$) (Table S28) < iA-3 ($1.09 \leq Q \leq 1.70$) (Table S34) < A-1 ($1.17 \leq Q \leq 1.54$) (Table S30 and Fig. S7 for comparative entropy-enthalpy compensation graphs). It is worth noting that the enantioseparations of compounds **1**-**6** with the systems C-1/A, C-1/E, A-1/E, iA-1/E, and iA-3

considered in the thermodynamic analysis were found to be enthalpy-driven ($Q > 1$) with the exception of the enantioseparation of compounds **1** and **2** with the system C-1/A, showing respectively entropy-driven ($Q < 1$) (T_{iso} = 7 °C) and mixed enthalpy/entropy-driven (T_{iso} = 35 °C) profiles (Fig. 5). For compounds **5** and **6** (compounds **1**-**3** were not enantioseparated with this column), the immobilized iA-1 showed lower Q values (Q = 1.29, 1.04) compared to the coated A-1 (Q = 1.54, 1.37). In accord with these results, T_{iso} values ranging from 52 °C to 233 °C were determined in almost all cases, whereas low T_{iso} values of 25 °C, 36 °C and 37 °C were found for **6** with systems C-1/E and iA-1/E, and for **2** with the system C-1/E, respectively. In general, it is expected that above the T_{iso} the EEO reverses compared to below it. However, in these three cases no EEO reversal was observed in the range 5-40 °C. In this regard, it is worth mentioning that, due to the chromatographic peak width, coelution may be observed in a certain temperature range around the T_{iso} [40].

As mentioned above, CSP backbone-dependent reversals of EEO was observed at 25 °C for compounds **5**, **6** and **7** by using mixture B as MP, moving from C-1 to A-1. In this case, it is likely that the size of both analytes and selector chiral cavities plays a role, **5** and **6** being the largest compounds of the ferrocene series (volume = 235.63 and 240.16 Å^3, respectively), and **7** the smallest (volume = 198.27 Å^3). Differently, for compound **1**, EEO reversal dependent on the CSP pendant group was observed under NP elution conditions (A) moving from C-1 (*R*-*S*) to iC-5 (*S*-*R*), and for compounds **1** and **3** in the aqueous methanol mixture E moving from A-1 (*S*-*R*) to iA-3 (*R*-*S*). In these cases, the balance between HBs, XBs and hydrophobic interactions could also play a role.

3.4. Effect of the mobile phase on the enantioseparation

The shape of the curves reported in Figures 3 and 4 suggested the presence of two sets of interactions underlying polar and hydrophobic mechanisms occurring respectively in hexane-based mixtures (A, B) and in aqueous mixtures (D, E). The impact of MP polarity on retention and selectivity appeared to be strictly dependent on analyte and CSP structures. The following trends could be observed:

295 *a)* in several cases, the use of pure MeOH as MP was detrimental for both polar and hydrophobic
296 mechanisms, and V-shaped curves centred on mixture C were obtained in these cases (Figs. 3a,b,c,d,g,h,j
297 and 4a,c,d,g);

298 *b)* MeOH, as a protic solvent, may participate in HBs with chiral selector, as well as with chiral
299 analyte, thus, in some cases application of this solvent was detrimental for analyte-selector polar
300 interactions resulting in decreased retention and selectivity moving from mixture A to B and C (Figs.
301 3a,b,d,e,g,h,j and 4a,d,g);

302 *c)* in other cases, the addition of few percentages of MeOH (B) tended to increase retention and
303 selectivity, likely favouring a better penetration of the analyte into the chiral groove (Figs. 3c,e,f,i,k,l and
304 4a,c-f,h,i,k,l);

305 *d)* the addition of water to methanol showed a variable impact on the enantioseparation depending on
306 analyte and CSP structure.

307 The thermodynamic differences between mixture A and E, in term of *Q*, were evaluated for column
308 C-1 and compounds **1**-**6**, showing a general increase of the $\Delta\Delta H°$ contribution to the $\Delta\Delta G°$ moving from
309 the hexane-based mixture ($1.00 \leq Q \leq 1.26$) to the aqueous methanol mixture ($1.17 \leq Q \leq 1.54$).

310 *3.5. Impact of analyte structure on the enantioseparation*

311 With the aim to evaluate the impact of the substitution pattern (1,2 vs 1,3), of the C≡C framework (–X
312 vs C≡C–X), and of the distinctive halogen type (F, Cl, Br) on the enantioseparability of compounds **1**-
313 **11**, the rate of baseline enantioseparations (*rbs*) at 25 °C was determined from the wealth of
314 chromatographic results. In the frame of the twenty-five chromatographic systems explored in this study
315 at 25°C, the *rbs* decreased following the order **10** (44%) > **11** (36%) > **5** (28%) > **6** (24%) > **4** (16%) >
316 **1**,**2** (12%) > **3** (8%) > **7**-**9** (0%). From this trend, some remarks emerged:

317 *a)* 1,3-disubstituted ferrocenes showed higher enantioseparability, in terms of *rbs*, compared to the
318 1,2-disubstituted analogues (**4**-**6** > **1**-**3** and **10**,**11** > **7**-**9**). Retention factors of **4**-**6** ($0.03 \leq k \leq 5.63$) and
319 **10**,**11** ($0.15 \leq k \leq 2.90$) were, in general, higher than those of **1**-**3** ($0.03 \leq k \leq 1.76$) and **7**-**9** ($0.14 \leq k \leq$

1.83), respectively. As first consideration, in the 1,3-disubstituted series more positive $V_{S,max}$ values (0.0466 au ≤ $V_{S,max}$ ≤0.0738 au) were calculated for the electrophilic σ-holes on halogens compared to the 1,2-disubstituted ferrocenes (0.0465 au ≤ $V_{S,max}$ ≤0.0721 au). In addition, both substituents are fully accessible to the selector in 1,3-disubstituted compounds, whereas the substituents are sterically constrained in 1,2-disubstituted derivatives. In the latter case, through-space contacts of adjacent electron charge density regions [31], associated with the main interaction sites, may contribute to limit the recognizability of the two enantiomers of the planar chiral ferrocenes. This structural feature could be confirmed by the fact that, in general, the SF percentage contribution to a V_S value from adjacent groups of the same type was higher for 1,2-disubstituted compounds compared to the 1,3-disubstituted ones. For instance, in compound **3**, the negative SF percentage contribution of the 2-iodoethynyl framework to the $V_{S,max}$ associated with the σ-hole of the 1-bromine atom is more negative (SF(I) + SF(C≡C) = -59.04%) compared to the same type of SF contribution calculated for 1,3-disubstituted ferrocene **6** (SF(I) + SF(C≡C) = -32.08%) (Table S9, Supplementary data). The same trend was observed for the SF(I) + SF(C≡C) values calculated for the pair **2** (-87.8%) and **5** (48.13%) (X = Cl), whereas a more positive contribution was determined for **1** (70.34%) compared to **4** (51.1%) (X = F). With the aim to understand correctly the meaning of the SF reconstruction, it is worth stressing that the SF contribution to the *V* in a point **r** depends on the electronic features of the contributing atom or groups as well as on the relative position between the contributing framework and the point **r** [31]. In addition, the sign of each contribution derives from the balance between nuclear and electronic contribution. Then, it is interesting to note the opposite contribution sign induced by the presence of the fluorine substituent (**1** and **4**) compared to the chlorinated (**2** and **5**) and brominated (**3** and **6**) compounds. On the basis of these differences, different chromatographic behaviours were expected for the fluorinated compounds compared to the chlorinated and brominated analogues.

Given that, compounds **1**-**3** provided baseline enantioseparations with higher α values (1.21 ≤ α ≤ 1.56) compared to compounds **4**-**6** (1.10 ≤ α ≤ 1.44) on amylose-based CSPs. In these cases, it is likely

that the more compact structure of 1,2-disubstituted ferrocenes may penetrate more easily in the compact chiral cavity of amylose-based selectors compared to the bigger 1,3-disubstituted ferrocenes. Moreover, in terms of HB acceptor properties, the $V_{S,min}$ associated with the ethynyl cloud is lower for compounds **1**-**3** (-0.0309 au ≤ $V_{S,min}$ ≤ -0.0327 au) compared to **4**-**6** (-0.0258 au ≤ $V_{S,min}$ ≤ -0.0266 au). The case of compound **8** proved also to be interesting due to the overlap between $V_{S,min}$ regions which are located in the negative belts of 1-chlorine and 2-iodine substituents of the ferrocenyl unit. This feature generates a region with a lower $V_{S,min}$ value ($V_{S,min}$ = -0.0251 au) (Supplementary data, Table S3) compared to the nucleophilic regions on the halogens in the analogues **7** ($V_{S,min}$ = -0.0109 au) and **9** ($V_{S,min}$ = -0.0113 au). This trend may justify the fact that **8** could be baseline enantioseparated, whereas partial enantioseparation was only achieved for **7** and **9**. The higher impact of 2-iodine atom on the adjacent 1-chlorine atom could be confirmed considering the SF contribution of iodine to the distinctive $V_{S,min}$ on halogens, which is more negative for **8** (SF(I) = -121.46%) compared to those of **11** (SF(I) = -68.72%), **7** (SF(I) = -72.70%) and **9** (SF(I) = -120.70%);

b) the ethynyl framework represents a key structural element which could exert a steric and an electronic impact on enantioseparation. The ethynyl π-cloud is a HB acceptor which may participate in HB with the amidic hydrogen of the selector and, as an EWG group, it activates the iodine σ-hole as electrophile. On the other hand, it induces a larger volume to the 1,3-disubstituted ferrocenes compared to the 1,2-disubstituted analogues. On this basis, the higher enantioseparability of compounds **1**-**3** (8% ≤ *rbs* ≤ 12%) compared to **7**-**9** (*rbs* = 0%) could be explained in terms of $V_{S,max}$ values associated to the electrophilic σ-hole on iodine. Indeed, the ethynyl group in **1**-**3** contributes to increase the electrophilic character of the iodine (0.0720 au ≤ $V_{S,max}$ (I) ≤ 0.0721 au) compared to the analogues **7**-**9** (0.0465 au ≤ $V_{S,max}$ (I) ≤ 0.0476 au). However, the opposite trend was observed for the 1,3-substituted derivatives **10** and **11** showing higher enantioseparability compared to **4** and **5**, respectively. In this case, the ethynyl framework could exert a detrimental effect on enantioseparability of **4** and **5**, in particular on iA-1, due to steric reasons;

c) the Cp system contributes to the hydrophobic character of the overall molecular system featuring compounds **1**-**11**, and it has also electron donor properties. However, functions of the Cp system at the molecular level are strongly modulated by the distinctive substitution of the ferrocenyl unit. In terms of *V* (Table S3, Supplementary data), the $V_{S,min}$ values in the unsubstituted Cp increase following the order F < Cl < Br and **1**-**3** < **4**-**6** ≈ **2**-**8** < **10**,**11**. For the substituted Cp ring, the variations related to halogen type are less important in terms of *V* variations, whereas, in this case, the $V_{S,min}$ values increase following the order **1**-**3** < **7**-**9** < **4**-**6** < **10**,**11**. Moreover, as shown in Table S13, the SF contribution of the distinctive halogens (X) to the $V_{S,min}$ associated to the Cp π-clouds is strongly type- and position-dependent for both substituted and unsubstituted Cp rings. In turn, the SF Cp system contribution to the halogen *V* values is variable in terms of sign and amount, also in this case depending on halogen type and position (Table S4-S12);

d) as shown in Figures 3 and 4, the impact of halogen type on the enantioseparation may be not easy to rationalize because the fine impact of CSP structure, MP polarity, and the other structural components of the analyte on the enantioseparation, as summarized above, is subtly dependent on steric and electronic properties, and position of F, Cl, and Br as distinctive substituents of compounds **1**-**11**. However, some hypotheses can be attempted on the basis of the comparative analyses of distinctive results.

3.6. Impact of halogen type on the enantioseparation

In most cases, retention of the analyte follows the order F < Cl < Br. This observation shows that the electrophilic features of the halogen or its hydrophobic character may drive retention. However, the higher electronegativity of fluorine proved to play a role in some cases. As mentioned above, the iC-5 enantioseparated compound **1**, exclusively by using A as MP. This result clearly relates this unique enantioseparation to the complementarity, in terms of HB recognition sites, between the CDCPC and **1**. Indeed, the amidic hydrogen of the CDCPC presents the highest $V_{S,max}$ value (0.0990 au) among the

394 selectors used in this study, namely the best properties as HB donor (Table S2), and compound **1**
395 features the most negative $V_{S,min}$ (-0.0347 au) observed in compounds **1**-**11** (Table S3).
396 The impact of the high electron density of fluorine may be also observed in the enantioseparation of
397 compounds **7**-**9** with the system A-1/B. In this case the selectivity factor decreases following the order F
398 ($\alpha = 1.10$) > Cl ($\alpha = 1.05$) > Br ($\alpha = 1.00$). However, it is worth noting that, in particular on the amylose-
399 based CSPs, the trend F > Cl > Br could be related to the steric hindrance of the halogens, increasing in
400 the opposite order Br > Cl > F. Indeed, the smaller fluorinated compounds should penetrate more easily
401 into the chiral cavities than its larger analogues.
402 An interesting trend emerges from the comparison of the impact of adding 2.5% MeOH in the
403 hexane/2-PrOH mixture A, obtaining the ternary mixture B, on the enantioseparation of compounds **1**-**3**
404 by using C-1. While for all compounds, retention decreased by adding 2.5% MeOH, the variations in
405 terms of selectivity factors were different. Indeed, α increased for compounds **1** ($\alpha_A = 1.06 \rightarrow \alpha_B = 1.08$)
406 and **2** ($\alpha_A = 1.00 \rightarrow \alpha_B = 1.07$), whereas it decreased for compound **3** ($\alpha_A = 1.16 \rightarrow \alpha_B = 1.00$).
407 Moreover, as mentioned above a reversal of EEO dependent on halogen type could be observed between
408 **1** (*R*-*S*) and **3** (*S*-*R*) with the system C1/A. As this trend revealed that diverse mechanisms could underlie
409 retention and selectivity, we evaluated comparatively the thermodynamic profiles of compounds **1**-**3** in
410 the range 5-40°C, with the chromatographic system C-1/A (Fig. 5). For compounds **1**-**3**, the T_{ISO} were
411 calculated from the thermodynamic quantities determined by classical van't Hoff equations as 7°C, 35°C
412 and 69°C. As mentioned above, at the T_{ISO}, the $\Delta\Delta H°$ and $\Delta\Delta S°$ terms contributing to the free energy
413 difference ($\Delta\Delta G°$) compensate each other, the free energy term is zero and the enantiomers co-elute. In
414 general, enantioseparations at lower temperatures than T_{ISO} are enthalpy-driven ($|\Delta H°| > |T\Delta S°|$), whereas
415 at higher temperatures enantioseparations are entropy-driven ($|\Delta H°| < |T\Delta S°|$). By changing the
416 temperature between the two regions, an EEO reversal occurs. On this basis, the thermodynamic profile
417 of the enantioseparation resulted entropic for compound **1**, containing F as distinctive halogen (Fig. 5a),
418 enthalpic for **3** (X = Br) (Fig. 5c), and a mixed entropic/enthalpic behaviour was obtained for **2** (X = Cl)

(Fig. 5b). For this latter enantioseparation, the EEO in the enthalpic domain was Y_2-X_2. In this regard, with the aim to verify the chromatographic behaviour in the region of the entropy domain, the enantioseparation of compound **2** was also performed at 45°C. Partial separation was observed at this temperature with the expected reversal of EEO (X_2-Y_2). For the structurally related compounds **1** and **3**, reversal of EEO was associated with two opposite thermodynamic profiles, *R*-*S* (**1**) in the entropy-driven domain, and *S*-*R* (**3**) in the enthalpy-driven domain. On this basis, due to its structural similarity to compounds **1** and **3**, for compound **2** it was reasonable to assign *S*-*R* to the undefined Y_2-X_2 in the enthalpic domain, and *R*-*S* to X_2-Y_2 in the entropic domain (Table 1). With the aim of identifying the distinctive recognition sites which produced different mechanisms at the molecular level, despite the similarity of the three compounds, $V_{S,min}$ and $V_{S,max}$ values on halogens were evaluated and compared. In this regard, *V* analysis showed that no relevant difference could be observed in compounds **1**-**3** in terms of *V* values of the cyclopentadienyl rings, iodine σ-holes and electronegative belts (Fig. 5d-f). Rather, 1-halogen atoms present major differences in terms of σ-hole and electronegative belt. Indeed, the σ-hole $V_{S,max}$ increases following the order F < Cl < Br as the polarizability of the halogens, whereas the $V_{S,min}$ on the halogen belt increases following the opposite order Br < Cl < F. Given that, the fluorine atom in compound **1** has higher electron density with a negative value of both $V_{S,min}$ (-0.0347 au) and $V_{S,max}$ (-0.0249 au) (Fig. 5d). Otherwise, the bromine atom, in compound **3**, has a more positive $V_{S,max}$ (0.0291 au) and a less negative $V_{S,min}$ (-0.0156 au) (Fig. 5f) compared to the chlorine atom in compound **2**, which presents intermediate values for chlorine $V_{S,min}$ (-0.0163 au) and $V_{S,max}$ (0.0189 au) (Fig. 5e). On this basis, it can be expected that HB involving the NH group of the selector as the HB donor participates in the enantiodifferentiation mechanism for the fluorinated compound **1**, whereas XB involving the carbonyl group of the selector for the more polarizable 1-bromo substituted compound **3**. Reasonably, in the first case, increasing temperature favours accommodation of the analyte into the groove, and the formation of the strong N–H···F–Fc (Fc = ferrocene) noncovalent interaction. In parallel, after complex formation, the entropy of the system increases, likely due to desolvation phenomena related to the

binding sites and to the hydrophobic feature of the analyte ($\Delta\Delta S°$ = 1.93, Q =0.94; EEO = *R*-*S*). In the case of compound **3**, given the higher positive $V_{S,max}$ on the bromine σ-hole, the enantioseparation is controlled by XB in an enthalpy-driven process ($\Delta\Delta S°$ = -1.91, Q =1.15; EEO = *S*-*R*). On the basis of the proposed model, as expected, by changing CDMPC to CDCPC (Fig. 6), an increase of the enantioseparation for the fluorinated compound (α_{CDMPC} = 1.06 → α_{CDCPC} = 1.09), and a decrease for the brominated system were observed (α_{CDMPC} = 1.16 → α_{CDCPC} = 1.00) due to the higher acidity of the NH and the higher $V_{S,min}$ value associated with the carbonyl oxygens in the chlorinated selector ($V_{S,min}$ (CDMPC) = -0.0625 au → $V_{S,min}$ (CDCPC) = -0.0536 au). By using mixture B as MP, the enantioseparation of compounds **2** (X = Cl), like compound **1** (X = F), is driven by the N–H···X–Fc interaction and, coherently, the EEO was *R*-*S* in both cases (Fig. 6). The EEO reversal in the enantioseparation of compound **1** observed upon changing C-1 to iC-5 could be rationalized through the interplay between the HB involving fluorine and the selector amidic hydrogen, and XB involving I as XB donor and the selector carbonyl oxygen. Given the lower XB acceptor power of the carbonyl oxygens in the CDCPC of iC-5, the XB is suppressed and the overall mechanism underlying retention and selectivity, and consequently EEO, changes. This mechanism does not occur within the series **4**-**6**, and only enthalpic thermodynamic profiles were derived in these cases.

Finally, the SF reconstruction of the V was applied to the $V_{S,max}$ and the $V_{S,min}$ associated with the halogen (F, Cl, Br) σ-holes and negative belts of compounds **1**-**3**. The reconstruction of the $V_{S,max}$ related to the iodine σ-hole (Fig. 7a) confirmed that no relevant differences in the atomic and group contributions from the components of the molecules occurred in compounds **1**-**3**. In particular, the decrease of the negative contribution from the distinctive halogen (green) was compensated by the decrease of the positive contribution from the substituted Cp (orange), resulting in a similar negative contribution from the Cp_{sub}-X groups to the $V_{S,max}$ (SF(X) + SF(substituted Cp) = -0.0163 au (**1**), -0.0173 au (**2**), -0.0175 au (**3**)) in all three cases. This analysis confirmed that the differences in the interaction modes within compounds **1**-**3** cannot be ascribed to the iodine σ-holes. On the contrary, different

patterns could be observed for the SF reconstruction of the $V_{S,max}$ and the $V_{S,min}$ associated with the distinctive halogen σ-holes (Fig. 7b) and negative belts (Fig. 7c). In particular, the Cp_{sub}-X group contributed to the negative $V_{S,max}$ of the fluorine atom in **1** (SF(X) + SF(substituted Cp) = -0.0638 au), whereas it opposes to the positive $V_{S,max}$ in **2** (SF(X) + SF(substituted Cp) = -0.0153 au) more than in **3** (SF(X) + SF(substituted Cp) = -0.0033 au), resulting in the more positive $V_{S,max}$ for the bromine atom compared to the chlorine atom. On the other hand, the SF(Cp_{sub}+X) contribution to the $V_{S,min}$ associated with the negative belt of the corresponding halogen increases following the order F (-0.0655 au) > Cl (-0.0633 au) > Br (-0.0625 au). In conclusion, for compounds **1**-**3** the comparison of the reconstruction results confirmed the SF origins of the electronic properties, described in terms of $V_{S,max}$ and $V_{S,min}$, which allowed for the rationalization of the enantioseparation mechanism as correlated with the experimental results.

4. Conclusions

In the enantioseparation of halogenated ferrocenes **1**-**11** on polysaccharide-based CSPs, retention and selectivity depend on a subtle balance between all possible functions and noncovalent interactions that the distinctive halogens may carry out and forms, respectively. Despite the fact that the presence of halogen atoms in a molecule increases its lipophilicity and hydrophobicity, halogens can also participate in polar noncovalent interactions. Thus, in principle, HB- and XB-based, hydrophobic and repulsive interaction modes can be switched on, switched off, or finely modulated depending on the structural features of analytes, halogens, CSPs, and MP polarity. In particular, the solvent components of the mobile phase can exert a pronounced effect on the overall structure and size of the chiral grooves within the polymeric network. Given that, mobile phase components may definitely play a role in determining the observed chromatographic outcomes through selective solvent-adsorption phenomena and by participating in solvation shells of all the interacting partners. As a result, in the enantioseparation of planar chiral halogenated ferrocenes, boundaries conditions have to be carefully selected as a function of halogen type and position in order to improve enantioseparation.

On this basis, the following practical guidelines can be provided to approach the enantioseparation of halogenated ferrocenes on polysaccharide-based CSPs: *a)* methylated and chloromethylated amylose-based columns exhibit better performances compared to cellulose-based columns; *b)* the rate of baseline enantioseparation of the immobilized iA-1 is lower compared to the coated A-1; *c)* temperature can be used as a parameter to optimize enantioseparation; *d)* methanol-containing mixtures provide better results in term of selectivity factors compared to classical *n*-hexane-2-propanol mixtures.

In most cases, retention followed the order F < Cl < Br which could be determined by the electrophilic σ-hole on the halogen atoms under NP conditions, as well as by hydrophobic contacts favoured in aqueous mixtures. However, it has been demonstrated that water may have little influence on the interaction energies and geometries of XB adducts in solution [54]. Consequently, XB can be considered as a hydrophobic equivalent of the hydrophilic HB [55], potentially also acting in water-containing MPs [28].

Thermodynamic profiles and EEO reversal dependent on halogen type were observed on CDMPC as selector. This phenomenon was explored at the molecular level by correlating experimental and computational data, and for this purpose, theoretical approaches such as *V* analyses and related SF reconstruction were successfully applied. Despite the fact that recognition mechanisms involving multiple noncovalent interactions may be challenging to deconvolute, integrating experimental and computational analysis represents a powerful tool to unravel the bases of enantioseparation mechanisms at the molecular level.

Acknowledgements

We thank the Consiglio Nazionale delle Ricerche (CNR), the University of Strasbourg and CNRS for financial support.

Appendix A. Supplementary data

Supplementary data associated with this article can be found, in the online version, at doi:

References

[1] T.J. Kealy, P.L. Pauson, A new type of organo-iron compound, Nature 168 (1951) 1039–1040. DOI: 10.1038/1681039b0

[2] S.A. Miller, J.A. Tebboth, J.F. Tremaine, 114. Dicyclopentadienyliron, J. Chem. Soc. (1952) 632–635. DOI: 10.1039/JR9520000632

[3] G. Wilkinson, M. Rosenblum, M.C. Whiting, R.B. Woodward, The structure of iron bis-cyclopentadienyl, J. Am. Chem. Soc. 74 (1952) 2125–2126. DOI:10.1021/ja01128a527

[4] E.O. Fischer, W. Pfab, Zur Kristallstruktur der Di-Cyclopentadienyl-Verbindungen des zweiwertigen Eisens, Kobalts und Nickels (On the crystal structure of the bis-cyclopentadienyl compounds of divalent iron, cobalt and nickel), Z. Naturforsch. B. 7 (1952) 377–379. DOI: 10.1515/znb-1952-0701

[5] P.F. Eilan, R. Pepinsky, X-ray examination of iron biscyclopentadienyl, J. Am. Chem. Soc. 74 (1952) 4971. DOI: 10.1021/ja01139a527

[6] D. Astruc, Why is ferrocene so exceptional? Eur. J. Inorg. Chem. (2017) 6–29. DOI: 10.1002/ejic.201600983

[7] M. Patra, G. Gasser, The medicinal chemistry of ferrocene and its derivatives, Nat. Rev. Chem. 1 (2017) 0066. DOI: 10.1038/s41570-017-0066

[8] L. Cunningham, A. Benson, P.J. Guiry, Recent developments in the synthesis and applications of chiral ferrocene ligands and organocatalysts in asymmetric catalysis, Org. Biomol. Chem. 18 (2020) 9329–9370. DOI: 10.1039/d0ob01933j

[9] A.N. Nesmeyanov, V.A. Sazonova, V.N. Drosd, Synthese von Ferrocenderivaten mittels bor- und halogensubstituierter Ferrocene, Chem. Ber. 93 (1960) 2717–2729. DOI: 10.1002/cber.19600931143

[10] J.W. Huffman, J.F. Cope, Reactions of 2-methylchloroferrocene. Evidence for the ferrocyne intermediate, J. Org. Chem. 36 (1971) 4068–4072. DOI: 10.1021/jo00825a013

[11] W.R. Cullen, S.J. Rettig, T.C. Zheng, Ferrocyne and ferrodicyne. Preparation and structures of $Os_3(CO)_9[\mu_3\text{-}(C_5H_3)Fe(C_5H_5)][\mu_3\text{-}P(C_5H_4)Fe(C_5H_5)]$, $Os_3(H)_2(CO)_8(PPr^i_2C_5H_2)Fe(C_5H_2PPr^i_2)Os_3(H)_2(CO)_8$, and $Os_3(CO)_9[\mu_3\text{-}C_6H_4][\mu_3\text{-}P(C_5H_4)Fe(C_5H_5)]$, Organometallics 11 (1992) 928−935. DOI: 10.1021/om00038a064

[12] H. Butenschön, Haloferrocenes: syntheses and selected reactions, Synthesis 50 (2018) 3787−3808. DOI: 10.1055/s-0037-1610210

[13] E. Aubert, A. Doudouh, E. Wenger, B. Sechi, P. Peluso, P. Pale, V. Mamane, Chiral ferrocenyl-iodotriazoles and -iodotriazoliums as halogen bond donors. Synthesis, solid state analysis and catalytic properties, Eur. J. Inorg. Chem. (2022) e202100927. DOI: 10.1002/ejic.202100927

[14] M. Wen, W. Erb, F. Mongin, Y.S. Halauko, O.A. Ivashkevich, V.E. Matulis, T. Roisnel, Synthesis of polysubstituted ferrocenesulfoxides, Molecules 27 (2022) 1798. DOI: 10.3390/molecules27061798

[15] V. Mamane, P. Peluso, E. Aubert, R. Weiss, E. Wenger, S. Cossu, P. Pale, Disubstituted ferrocenyl iodo- and chalcogenoalkynes as chiral halogen and chalcogen bond donors, Organometallics 39 (2020) 3936−3950. DOI: 10.1021/acs.organomet.0c00633

[16] L.–X. Dai, T. Tu, S.–L. You, W.–P. Deng, X.–L. Hou, Asymmetric catalysis with chiral ferrocene ligands, Acc. Chem. Res. 36 (2003) 659–667. DOI: 10.1021/ar020153m

[17] O. Riant, G. Argouarch, D. Guillaneux, O. Samuel, H.B. Kagan, A straightforward asymmetric synthesis of enantiopure 1,2-disubstituted ferrocenes, J. Org. Chem. 63 (1998) 3511–3514. DOI: 10.1021/jo9800614

[18] F. Rebière, O. Riant, L. Ricard, H.B. Kagan, Asymmetric synthesis and highly diastereoselective ortho-lithiation of ferrocenyl sulfoxides. Application to the synthesis of ferrocenyl derivatives with planar chirality, Angew. Chem. Int. Ed. Engl. 32 (1993) 568–570. DOI: 10.1002/anie.199305681

[19] R.A. Thorat, S. Jain, M. Sattar, P. Yadav, Y. Mandhar, S. Kumar, Synthesis of chiral-substituted 2-aryl-ferrocenes by the Catellani reaction, J. Org. Chem. 85 (2020) 14866−14878. DOI: 10.1021/acs.joc.0c01360

[20] M. Tsukazaki, M. Tinkl, A. Roglans, B.J. Chapell, N.J. Taylor, V. Snieckus, Direct and highly enantioselective synthesis of ferrocenes with planar chirality by (-)-sparteine-mediated lithiation, J. Am. Chem. Soc. 118 (1996) 685–686. DOI: /10.1021/ja953246q

[21] W. Erb, M. Wen, J. P. Hurvois, F. Mongin, Y.S. Halauko, O.A. Ivashkevich, V.E. Matulis, T. Roisnel, *O*-Isopropylferrocenesulfonate: synthesis of polysubstituted derivatives and electrochemical study, Eur. J. Inorg. Chem. (2021) 3165–3176. DOI: 10.1002/ejic.202100448

[22] Y. Yamazaki, N. Morohashi, K. Hosono, High-performance liquid chromatographic determination of optical purity of planar chiral organometallic compounds resolved by enzymic transformations, J. Chromatogr. A 542 (1991) 129−136. DOI: 10.1016/S0021-9673(01)88753-7

[23] A. Patti, S. Pedotti, C. Sanfilippo, Comparative HPLC enantioseparation of ferrocenylalcohols on two cellulose-based chiral stationary phases, Chirality 19 (2007) 344-351. DOI: 10.1002/chir.20386

[24] M. Ogasawara, Y. Enomoto, M. Uryu, X. Yang, A. Kataoka, A. Ohnishi, Application of polysaccharide-based chiral HPLC columns for separation of nonenantiomeric isomeric mixtures of organometallic compounds, Organometallics 38 (2019) 512−518. DOI: 10.1021/acs.organomet.8b00819

[25] A. Dessì, B. Sechi, R. Dallocchio, B. Chankvetadze, M. Pérez-Baeza, S. Cossu, V. Mamane, P. Pale, P. Peluso, Comparative enantioseparation of planar chiral ferrocenes on polysaccharide-based chiral stationary phases, Chirality 34 (2022) 609−619. DOI: 10.1002/chir.23417

[26] P. Peluso, V. Mamane, S. Cossu, Liquid chromatography enantioseparations of halogenated compounds on polysaccharide-based chiral stationary phases: role of halogen substituents in molecular recognition. Chirality 27 (2015), 667–684. DOI: 10.1002/chir.22485

[27] P. Peluso, V. Mamane, E. Aubert, A. Dessì, R. Dallocchio, A. Dore, P. Pale, S. Cossu, Insights into halogen bond-driven enantioseparations, J. Chromatogr. A 1467 (2016) 228–238. DOI: 10.1016/j.chroma.2016.06.007

[28] P. Peluso, V. Mamane, R. Dallocchio, A. Dessì, R. Villano, D. Sanna, E. Aubert, P. Pale, S. Cossu, Polysaccharide-based chiral stationary phases as halogen bond acceptors: A novel strategy for detection of stereoselective σ-hole bonds in solution, J. Sep. Sci. 41 (2018) 1247–1256. DOI: 10.1002/jssc.201701206

[29] P. Peluso, B. Chankvetadze, The molecular bases of chiral recognition in 2-(benzylsulfinyl)benzamide enantioseparation, Anal. Chim. Acta 1141 (2021) 194–205. DOI: 10.1016/j.aca.2020.10.050

[30] C. Gatti, The source function descriptor as a tool to extract chemical information from theoretical and experimental electron densities, Struct. Bond. 147 (2012) 193–286. DOI: 10.1007/430_2010_31

[31] C. Gatti, A. Dessì, R. Dallocchio, V. Mamane, S. Cossu, R. Weiss, P. Pale, E. Aubert, P. Peluso, Factors impacting σ- and π-hole regions as revealed by the electrostatic potential and its source function reconstruction: The case of 4,4'-bipyridine derivatives, Molecules 25 (2020) 4409. DOI: 10.3390/molecules25194409

[32] P. Peluso, A. Dessì, R. Dallocchio, B. Sechi, C. Gatti, B. Chankvetadze, V. Mamane, R. Weiss, P. Pale, E. Aubert, S. Cossu, Enantioseparation of 5,5'-dibromo-2,2'-dichloro-3-selanyl-4,4'-bipyridines on polysaccharide-based chiral stationary phases: exploring chalcogen bonds in liquid-phase chromatography, Molecules 26 (2021) 221. DOI: 10.3390/molecules26010221

[33] P. Peluso, C. Gatti, A. Dessì, R. Dallocchio, R. Weiss, E. Aubert, P. Pale, S. Cossu, V. Mamane, Enantioseparation of fluorinated 3-arylthio-4,4'-bipyridines: insights into chalcogen and π-hole bonds in high-performance liquid chromatography, J. Chromatogr. A 1567 (2018) 119–129. DOI: 10.1016/j.chroma.2018.06.060

[34] M. Tazi, M. Hedidi, W. Erb, Y.S. Halauko, O.A. Ivashkevich, V.E. Matulis, T. Roisnel, V. Dorcet, G. Bentabed-Ababsa, F. Mongin, Fluoro- and chloroferrocene: from 2- to 3-substituted derivatives, Organometallics 37 (2018) 2207−221. DOI: 10.1021/acs.organomet.8b00384

[35] M. Tazi, W. Erb, T. Roisnel, V. Dorcet, F. Mongin, P.J. Low, From ferrocene to fluorine-containing pentasubstituted derivatives and all points in-between; or, how to increase the available chemical space, Org. Biomol. Chem. 17 (2019) 9352–9359. DOI: 10.1039/c9ob01885a

[36] G. Dayaker, A. Sreeshailam, F. Chevallier, T. Roisnel, P.R. Krishna, F. Mongin, Deprotonative metallation of ferrocenes using mixed lithium−zinc and lithium−cadmium combinations, Chem. Commun. 46 (2010) 2862−2864. DOI: 10.1039/B924939G

[37] M.J. Frisch, G.W. Trucks, H.B. Schlegel, G.E. Scuseria, M.A. Robb, J.R. Cheeseman, G. Scalmani, V. Barone, B. Mennucci, G.A. Petersson, H. Nakatsuji, M. Caricato, X. Hratchian, H.P. Li, A.F. Izmaylov, J. Bloino, G. Zheng, J.L. Sonnenberg, M. Hada, M. Ehara, K. Toyota, R. Fukuda, J. Hasegawa, M. Ishida,T. Nakajima, Y. Honda, O. Kitao, H. Nakai, T. Vreven, J.A. Montgomery Jr., J.E. Peralta, F. Ogliaro, M. Bearpark, J.J. Heyd, E. Brothers, K.N. Kudin, V.N. Staroverov, T. Keith, R. Kobayashi, J. Normand, K. Raghavachari, A. Rendell, J.C. Burant, S.S. Iyengar, J. Tomasi, M. Cossi, N. Rega, J.M. Millam, M. Klene, J.E. Knox, J.B. Cross, V. Bakken, C. Adamo, J. Jaramillo, R. Gomperts, R.E. Stratmann, O. Yazyev, A.J. Austin, R. Cammi, C. Pomelli, J.W. Ochterski, R.L. Martin, K. Morokuma, V.G. Zakrzewski, G. Voth, P. Salvador, J.J. Dannenberg, S. Dapprich, A.D. Daniels, O. Farkas, J.B. Foresman, J. Ortiz, J. Cioslowski, D.J. Fox, Gaussian 09, Revision B. 01, Inc.Gaussian, C.T. Wallingford, 2010.

[38] T. Lu, F. Chen, Multiwfn: A multifunctional wavefunction analyser. J. Comp. Chem. 33 (2012) 580–592. DOI: 10.1002/jcc.22885

[39] T. Lu, F. Chen, Quantitative analysis of molecular surface based on improved Marching Tetrahedra algorithm. J. Mol. Graph. Model. 38 (2012) 314–323. DOI: 10.1016/j.jmgm.2012.07.004

[40] B. Chankvetadze, Recent trends in preparation, investigation and application of polysaccharide-based chiral stationary phases for separation of enantiomers in high-performance liquid chromatography, Trends Anal. Chem. 122 (2020) 115709. DOI: 10.1016/j.trac.2019.115709

[41] P. Peluso, B. Sechi, G. Lai, A. Dessì, R. Dallocchio, S. Cossu, E. Aubert, R. Weiss, P. Pale, V. Mamane, B. Chankvetadze, Comparative enantioseparation of chiral 4,4'-bipyridine derivatives on coated and immobilized amylose-based chiral stationary phases, J. Chromatogr. A. 1625 (2020) 461303. DOI: 10.1016/j.chroma.2020.461303

[42] B. Chankvetadze, C. Yamamoto, Y. Okamoto, Enantioseparation of selected chiral sulfoxides using polysaccharide-type chiral stationary phases and polar organic, polar aqueous–organic and normal-phase eluents, J. Chromatogr. A. 922 (2001) 127–137. DOI: 10.1016/S0021-9673(01)00958-X

[43] B. Chankvetadze, Recent developments on polysaccharide-based chiral stationary phases for liquid-phase separation of enantiomers, J. Chromatogr. A. 1269 (2012) 26–51. DOI: 10.1016/j.chroma.2012.10.033

[44] M. Dobó, M. Foroughbakhshfasaei, P. Horváth, Z.–I. Szabó, G. Tóth, Chiral separation of oxazolidinone analogues by liquid chromatography on polysaccharide stationary phases using polar organic mode, J. Chromatogr. A. 1662 (2022) 462741. DOI: 10.1016/j.chroma.2021.462741

[45] Z. Shedania, R. Kakava, A. Volonterio, T. Farkas, B. Chankvetadze, Separation of enantiomers of chiral sulfoxides in high-performance liquid chromatography with cellulose-based chiral selectors using methanol and methanol-water mixtures as mobile phases, J. Chromatogr A. 1557 (2018) 62–74. DOI: 10.1016/j.chroma.2018.05.002

[46] A. Bondi, van der Waals volume and radii, J. Phys. Chem. 68 (1964) 441–451. DOI: 10.1021/j100785a001

[47] A. Singh, I. Lumb, V. Mehra, V. Kumar, Ferrocene-appended pharmacophores: an exciting approach for modulating the biological potential of organic scaffolds, Dalton Trans. 48 (2019) 2840–2860. DOI: 10.1039/c8dt03440k

[48] C. Gatti, F. Cargnoni, L. Bertini, Chemical information from the source function, J. Comput. Chem. 24 (2003) 422–436. DOI: 10.1002/jcc.10205

[49] I. Matarashvili, G. Kobidze, A. Chelidze, G. Dolidze, N. Beridze, G. Jibuti, T. Farkas, B. Chankvetadze, The effect of temperature on the separation of enantiomers with coated and covalently immobilized polysaccharide-based chiral stationary phases, J. Chromatogr. A 1599 (2019) 172–179. DOI: 10.1016/j.chroma.2019.04.024

[50] F. Ianni, Z. Pataj, H. Gross, R. Sardella, B. Natalini, W. Lindner, M. Lämmerhofer, Direct enantioseparation of underivatized aliphatic 3-hydroxyalkanoic acids with a quinine-based zwitterionic chiral stationary phase, J. Chromatogr. A 1363 (2014) 101–108. DOI: 10.1016/j.chroma.2014.03.060

[51] P. Peluso, V. Mamane, R. Dallocchio, A. Dessì, S. Cossu, Noncovalent interactions in high-performance liquid chromatography enantioseparations on polysaccharide-based chiral selectors, J. Chromatogr. A 1623 (2020) 461202. DOI: 1016/j.chroma.2020.461202.

[52] T. Fornstedt, Characterization of adsorption processes in analytical liquid–solid chromatography, J. Chromatogr. A 1217 (2010) 792–812. DOI: 10.1016/j.chroma.2009.12.044

[53] D. Tanács, T. Orosz, Z. Szakonyi, T.M. Le, F. Fülöp, W. Lindner, I. Ilisz, A. Péter, High-performance liquid chromatographic enantioseparation of isopulegol-based ß-amino lactone and ß-amino amide analogs on polysaccharide-based chiral stationary phases focusing on the change of the enantiomer elution order, J. Chromatogr. A 1621 (2020) 461054. DOI: 10.1016/j.chroma.2020.461054

687 [54] Y. Lu, H. Li, X. Zhu, W. Zhu, H. Liu, How does halogen bonding behave in solution? A
688 theoretical study using implicit solvation model, J. Phys. Chem. A 115 (2011) 4467–4475. DOI:
689 10.1021/jp111616x
690 [55] A. Priimagi, G. Cavallo, P. Metrangolo, G. Resnati, The halogen bond in the design of functional
691 supramolecular materials: recent advances, Acc. Chem. Res. 46 (2013) 2686–2695. DOI:
692 10.1021/ar400103r
693

FIGURE CAPTIONS

Fig. 1. Structures and numbering of halogenated chiral ferrocenes **1-11**.

Fig. 2. *V* isosurface (0.002 au) of compound **2**, as a representative analyte, showing the main interaction sites of the molecular systems featuring compounds **1-11** (colour legend: red, high electron charge density regions; blue, regions of electron charge density depletion; orange, yellow, green, and pale blue describes intermediate regions of electron charge density between the two extrema (red and blue regions).

Fig. 3. Comparison of retention factor of the first eluted enantiomers (k_1) of compounds **1-11** on chiral columns C-1 (a, d, g, j), A-1 (b, e, h, k), and iA-3 (c, f, i, l) under multimodal elution conditions (A, Hex/2-PrOH 95:5 v/v; B, Hex/2-PrOH/MeOH 95:2.5:2.5 v/v/v; C, MeOH 100%; D, MeOH/water 95:5 v/v; E, MeOH/water 90:10 v/v).

Fig. 4. Comparison of selectivity factors (α) of compounds **1-11** on chiral columns C-1 (a, d, g, j), A-1 (b, e, h, k), and iA-3 (c, f, i, l) under multimodal elution conditions (A, Hex/2-PrOH 95:5 v/v; B, Hex/2-PrOH/MeOH 95:2.5:2.5 v/v/v; C, MeOH 100%; D, MeOH/water 95:5 v/v; E, MeOH/water 90:10 v/v).

Fig. 5. Enantioseparation of compounds **1** (a), **2** (b), and **3** (c) at variable temperature on C-1 with mixture A, and variation of the $V_{S,min}$ and $V_{S,max}$ values (d-f) as the 1-halogen substituent changes in the series of 1-halo-2-(iodoethynyl)ferrocenes **1-3**.

Fig. 6. Comparative enantioseparation of compounds **1** (a), **2** (b), and **3** (c) (T = 25°C) by using the chromatographic system C-1/A (blue), iC-5/A (red), and C-1/B (green).

Fig. 7. Iodine σ-hole $V_{S,max}$ (a), and halogen (X = F, Cl, Br) $V_{S,max}$ (b) and and $V_{S,min}$ (c) Source Function reconstruction for compounds **1**, **2**, and **3** (see Supplementary data, Tables S4-S12 for complete data).

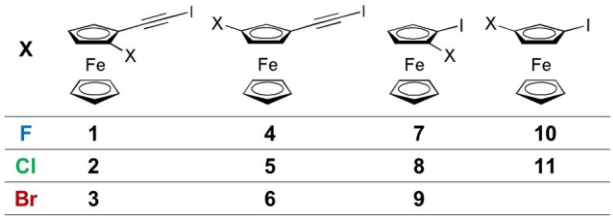

716

717 **Fig. 1.** Structures and numbering of halogenated chiral ferrocenes **1-11**.

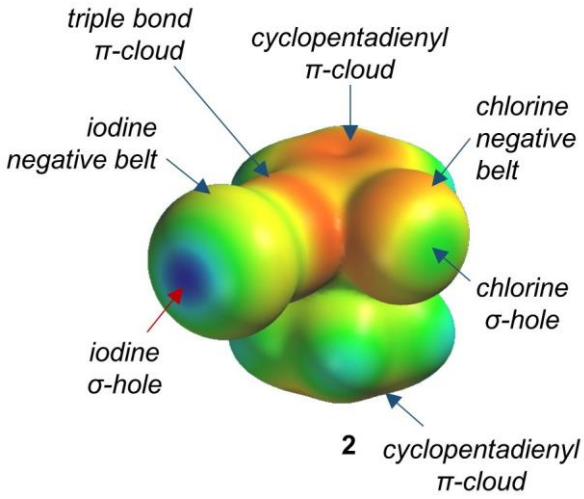

718

719 **Fig. 2.** *V* isosurface (0.002 au) of compound **2**, as a representative analyte, showing the main interaction
720 sites of the molecular systems featuring compounds **1-11** (colour legend: red, high electron charge
721 density regions; blue, regions of electron charge density depletion; orange, yellow, green, and pale blue
722 describes intermediate regions of electron charge density between the two extrema (red and blue
723 regions).

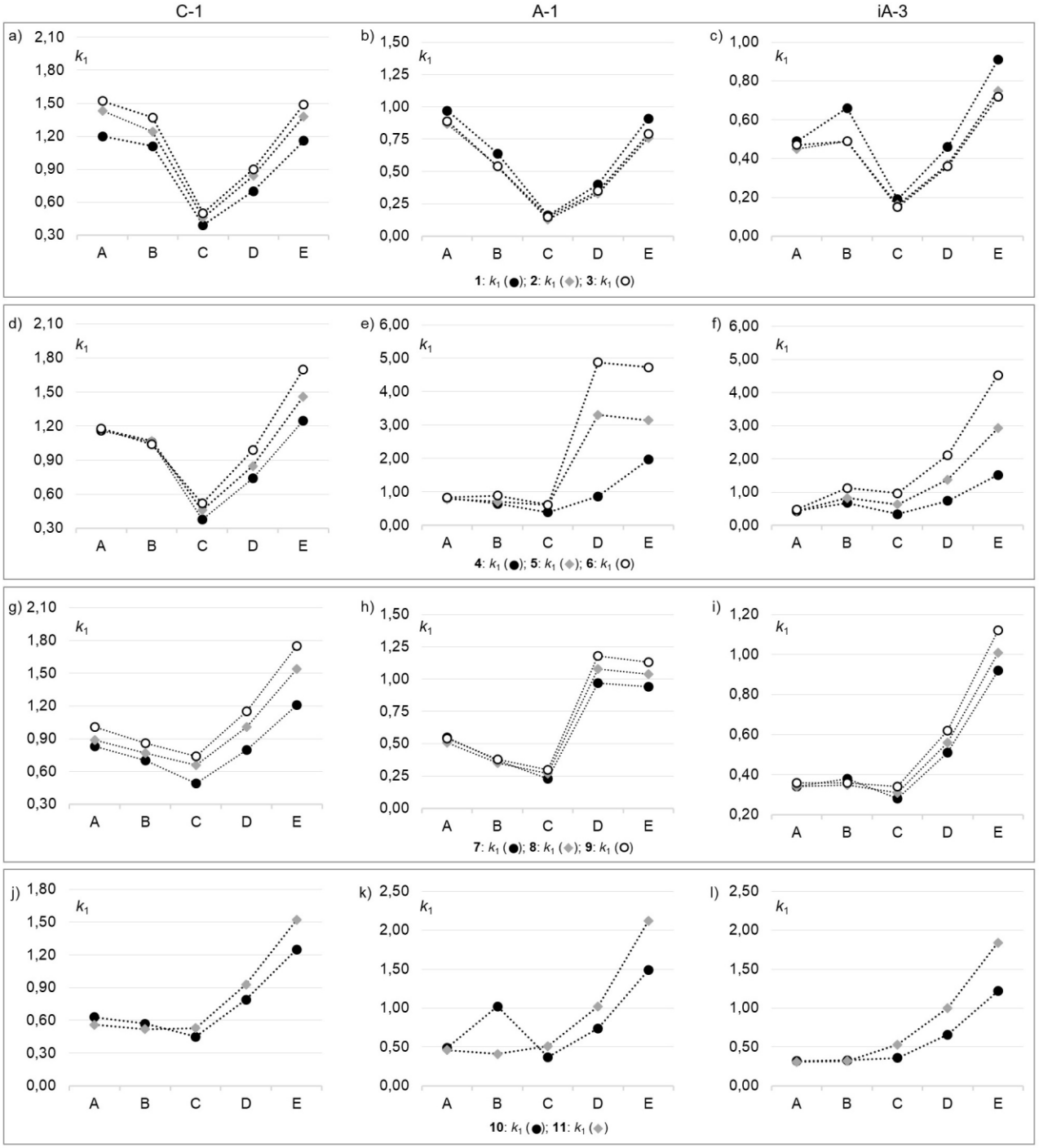

724

725 **Fig. 3.** Comparison of retention factor of the first eluted enantiomers (k_1) of compounds **1-11** on chiral
726 columns C-1 (a, d, g, j), A-1 (b, e, h, k), and iA-3 (c, f, i, l) under multimodal elution conditions (A,
727 Hex/2-PrOH 95:5 v/v; B, Hex/2-PrOH/MeOH 95:2.5:2.5 v/v/v; C, MeOH 100%; D, MeOH/water 95:5
728 v/v; E, MeOH/water 90:10 v/v).

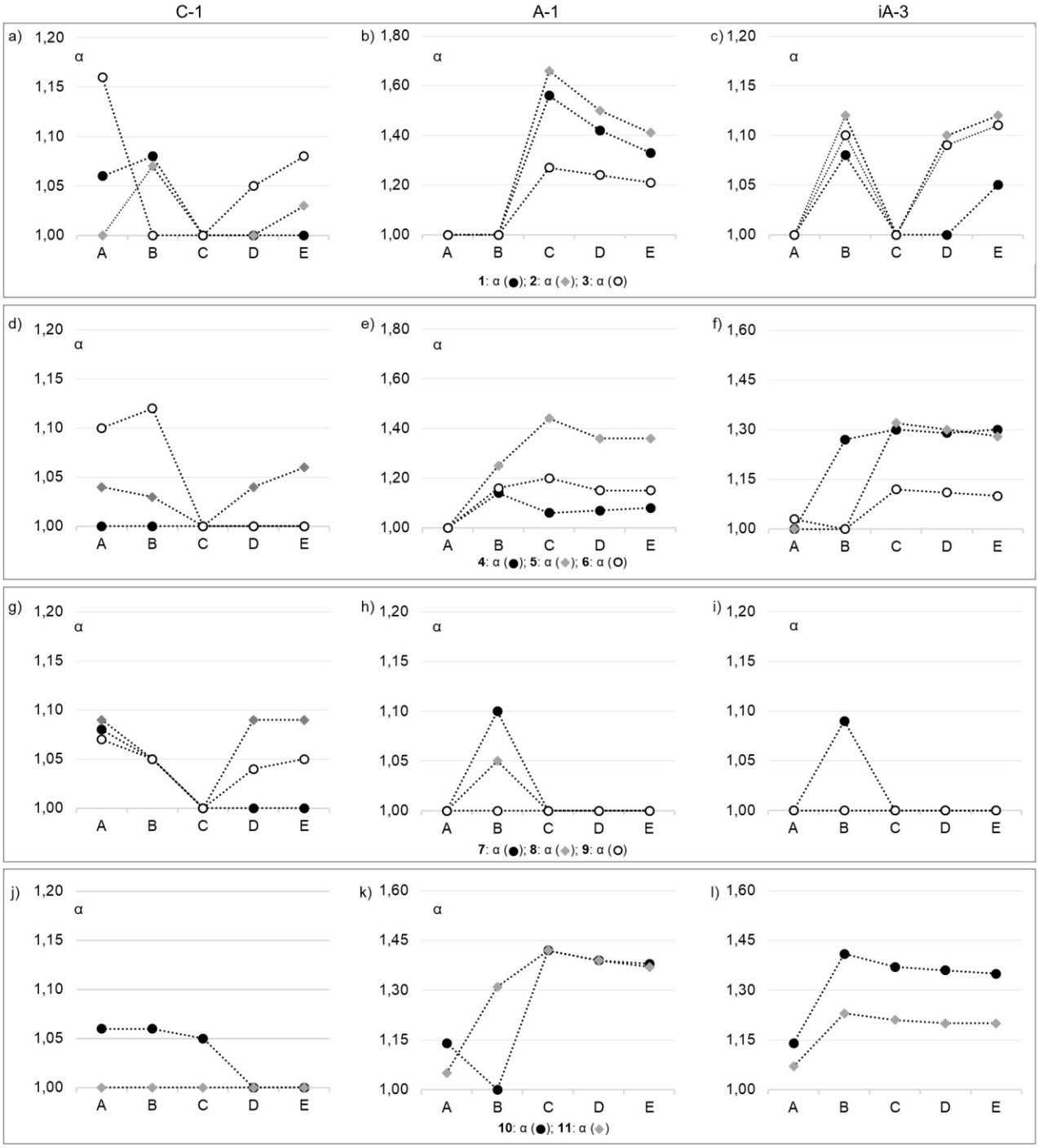

729

730 **Fig. 4.** Comparison of selectivity factors (α) of compounds **1-11** on chiral columns C-1 (a, d, g, j), A-1

731 (b, e, h, k), and iA-3 (c, f, i, l) under multimodal elution conditions (A, Hex/2-PrOH 95:5 v/v; B, Hex/2-

732 PrOH/MeOH 95:2.5:2.5 v/v/v; C, MeOH 100%; D, MeOH/water 95:5 v/v; E, MeOH/water 90:10 v/v).

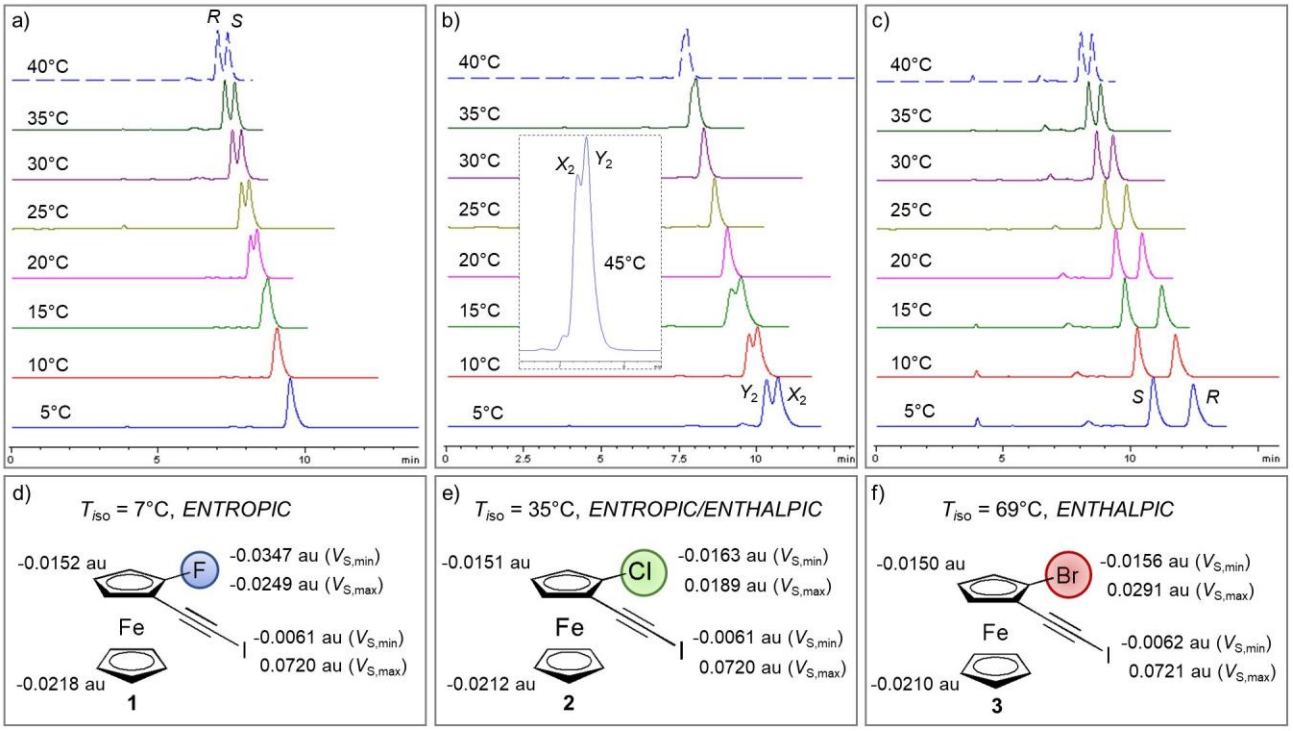

Fig. 5. Enantioseparation of compounds **1** (a), **2** (b), and **3** (c) at variable temperature on C-1 with mixture A, and variation of the $V_{S,min}$ and $V_{S,max}$ values (d-f) as the 1-halogen substituent changes in the series of 1-halo-2-(iodoethynyl)ferrocenes **1**-**3**.

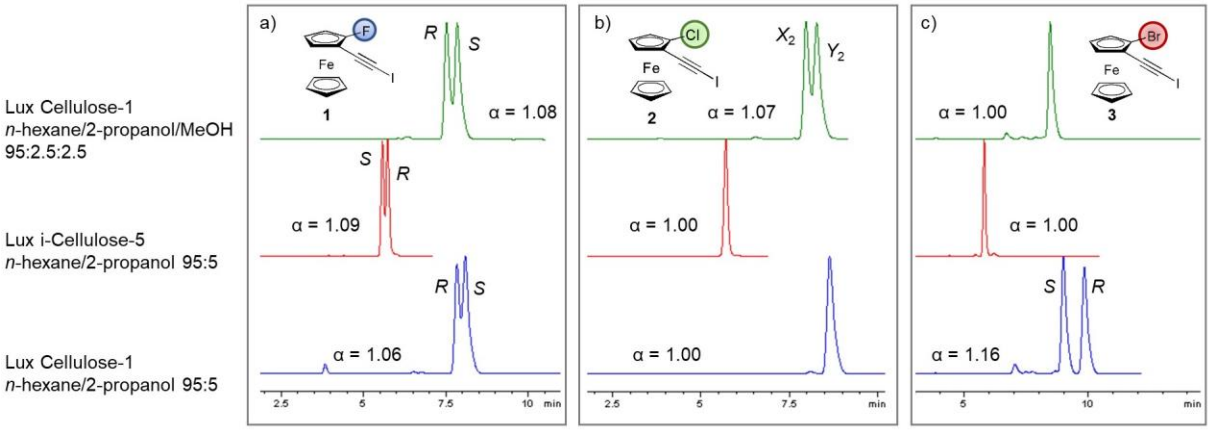

Fig. 6. Comparative enantioseparation of compounds **1** (a), **2** (b), and **3** (c) (T = 25°C) by using the chromatographic system C-1/A (blue), iC-5/A (red), and C-1/B (green).

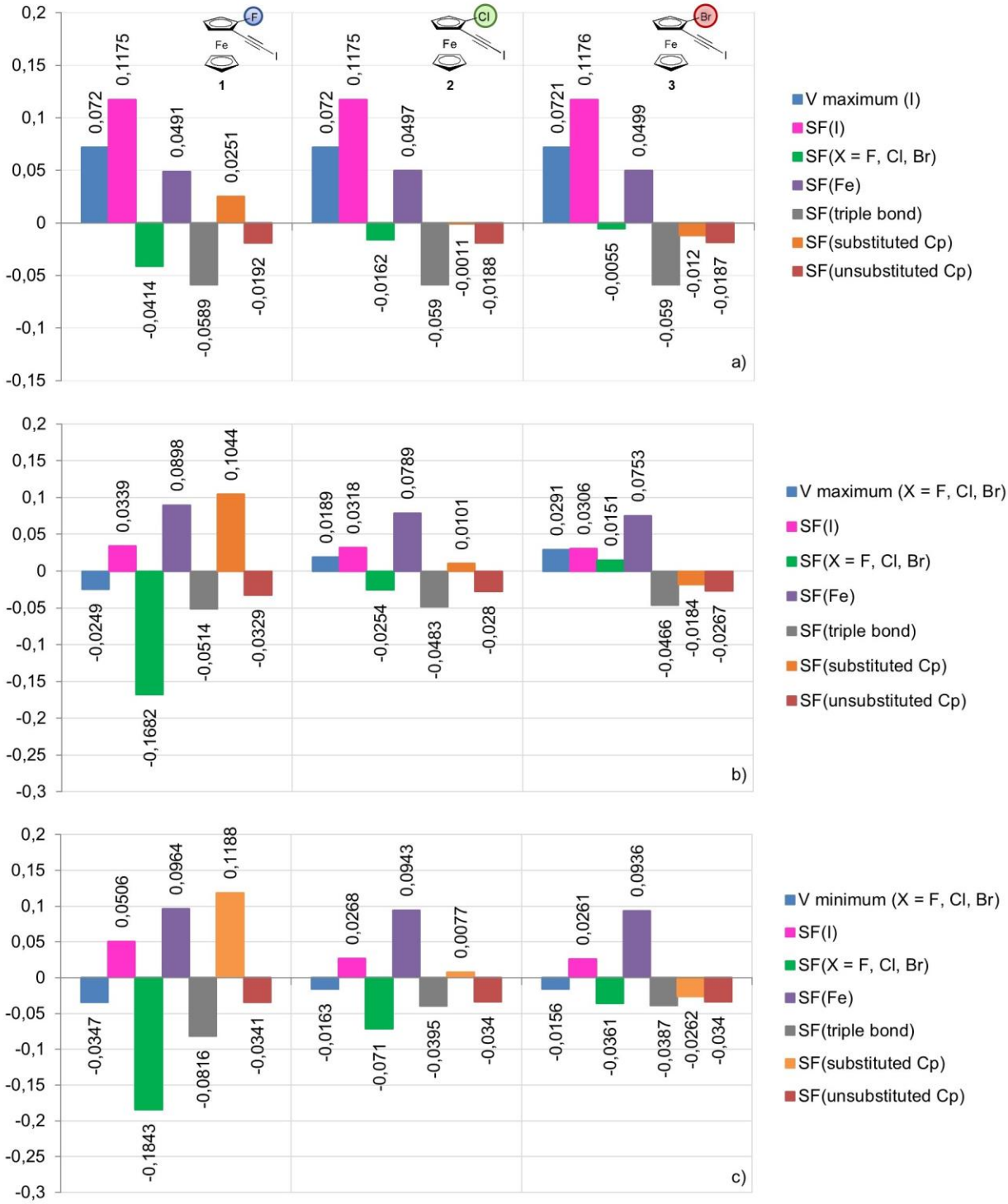

Fig. 7. Iodine σ-hole $V_{S,max}$ (a), and halogen (X = F, Cl, Br) $V_{S,max}$ (b) and and $V_{S,min}$ (c) Source Function reconstruction for compounds **1**, **2**, and **3** (see Supplementary data, Tables S4-S12 for complete data).